JACS
JOURNAL OF THE AMERICAN CHEMICAL SOCIETY
Article
pubs.acs.org/JACS

Hydrogen Atom Abstraction from Hydrocarbons by a Copper(III)-Hydroxide Complex

Debanjan Dhar and William B. Tolman*

Department of Chemistry and Center for Metals in Biocatalysis, University of Minnesota, 207 Pleasant Street SE, Minneapolis, Minnesota 55455, United States

Supporting Information

ABSTRACT: With the aim of understanding the basis for the high rate of hydrogen atom abstraction (HAT) from dihydroanthracene (DHA) by the complex LCuOH (**1**; L = *N*,*N*′-bis(2,6-diisopropylphenyl)-2,6-pyridinedicarboxamide), the bond dissociation enthalpy of the reaction product LCu(H$_2$O) (**2**) was determined through measurement of its pK_a and $E_{1/2}$ in THF solution. In so doing, an equilibrium between **2** and LCu(THF) was characterized by UV−vis and EPR spectroscopy and cyclic voltammetry (CV). A high pK_a of 18.8 ± 1.8 and a low $E_{1/2}$ of −0.074 V vs Fc/Fc$^+$ in THF combined to yield an O−H BDE for **2** of 90 ± 3 kcal mol^{-1} that is large relative to values for most transition metal oxo/hydroxo complexes. By taking advantage of the increased stability of **1** observed in 1,2-difluorobenzene (DFB) solvent, the kinetics of the reactions of **1** with a range of substrates with varying BDE values for their C−H bonds were measured. The oxidizing power of **1** was revealed through the accelerated decay of **1** in the presence of the substrates, including THF (BDE = 92 kcal mol^{-1}) and cyclohexane (BDE = 99 kcal mol^{-1}). CV experiments in THF solvent showed that **1** reacted with THF via rate-determining attack at the THF C−H(D) bonds with a kinetic isotope effect of 10.2. Analysis of the kinetic and thermodynamic data provides new insights into the basis for the high reactivity of **1** and the possible involvement of species like **1** in oxidation catalysis.

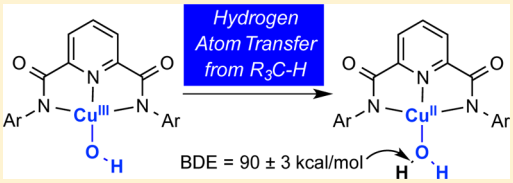

INTRODUCTION

Understanding the properties of copper−oxygen intermediates proposed for oxidations catalyzed by copper enzymes[1] and other systems is critical for gaining mechanistic insights and developing new catalytic processes. Extensive studies of reactions of O_2 and other oxidants with copper complexes has led to the identification of a number of important copper−oxygen species relevant to metalloenzyme and other catalytic intermediates.[2] Nonetheless, much needs to be done via synthetic chemistry approaches to evaluate provocative proposals for motifs involved in oxidation catalysis, such as the [CuO]$^+$ moiety in monocopper systems[2c,3] or the mixed-valent Cu^{II}−O$_n$−Cu^{III} units (n = 1 or 2) proposed for particulate methane monoxygenase.[4] Recently, we reported[5] the synthesis and characterization of novel complexes with a [CuOH]$^{2+}$ core (**1**, R = *i*Pr or Me; Scheme 1) that can be viewed as a protonated form of the elusive [CuO]$^+$ unit.[6] Aspects of the reactivity of **1** attest to the viability of the [CuOH]$^{2+}$ core as a potential reactive intermediate in oxidation catalysis, such as the rapid reaction with dihydroanthracene (DHA) to yield anthracene and the aquo complex **2** (for R = *i*Pr, k = 1−24 M^{-1} s^{-1} from −80 to −30 °C).[5a] This second order reaction features a large kinetic isotope effect (k_H/k_D = 44 at −70 °C) consistent with a rate-determining hydrogen atom abstraction (HAT) mechanism. The rapid rate of HAT is particularly intriguing in view of the fact that **1** is a weak oxidant[5a] (for R = *i*Pr, $E_{1/2}$ = −0.076 V vs Fc$^+$/Fc in acetone).[7]

To place the properties of **1** in perspective, it is informative to draw comparisons to other metal-oxo or -hydroxo complexes from the first transition series. A number of such complexes with iron and manganese, for example, have been prepared and their reactivity with substrate C−H bonds examined in efforts to understand intrinsic properties and evaluate feasibility as catalytic intermediates.[7,8] Important mechanistic insights have been obtained in these studies through evaluation of the reaction thermodynamics, in particular the measurement of the bond dissociation enthalpy (BDE) or free energy (BDFE) of the O−H bond formed in the product complex. As described in

Scheme 1

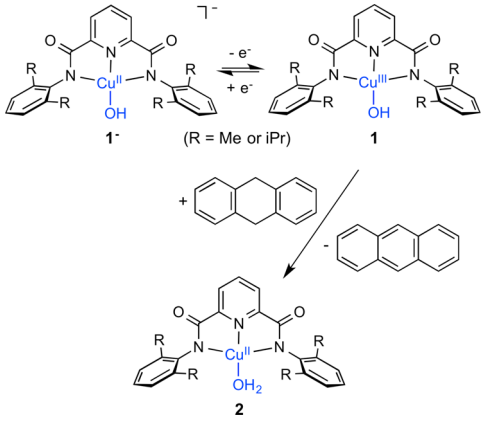

Received: November 24, 2014
Published: January 12, 2015

DOI: 10.1021/ja512014z
J. Am. Chem. Soc. 2015, 137, 1322−1329

detail elsewhere,[9,10] the BDE or BDFE may be determined using Hess' law and a square scheme from the redox potential and the pK_a associated with the HAT process (eq 1, where C_H is a constant associated with the $H^+/H^\bullet$ standard reduction potential). Correlations of the BDE/BDFE with reaction rates (i.e., log k vs BDE plots) and evaluations of the interplay of redox potential and pK_a that underly the BDE/BDFE values have been shown to be especially informative.[7,9]

$$\mathrm{BDE} = 1.37\mathrm{p}K_a + 23.06E^\circ + C_H \quad (1)$$

Herein, we report the results of efforts to apply the aforementioned methodologies to **1** (R = *i*Pr, from this point onward), with the aim of understanding the basis for the HAT rates observed and evaluating the potential for reactivity with substrates with stronger C−H bonds than DHA (BDE = 76 kcal mol^{-1}).[11] We have succeeded in determining the BDE of the O−H bond in **2**, and discuss this value in terms of experimental evaluations of redox potential and basicity. Comparisons of the thermodynamic properties of the **1**/**2** system are drawn to previous results for a range of metal-oxo/hydroxo complexes. In addition, we discovered that **1** attacks the C−H bonds of THF and other substrates with C−H BDE values >80 kcal mol^{-1}, and preliminary mechanistic information on these reactions are presented. Together, the results of these studies provide important fundamental insights into the properties of the $[CuOH]^{2+}$ moiety, which support the notion that it may be considered as a feasible reactive intermediate in oxidation catalysis.

RESULTS

Thermodynamics. In order to determine the BDE for the O−H bond in **2** experimentally, we referred to the square scheme shown in Figure 1. Because species **1**$^-$, **1**, and **2** (R = *i*Pr) had been characterized previously, the BDE was targeted through determination of p$K_{a(1)}$, E°_1 (approximated as $E_{1/2}$ for the **1**$^-$/**1** couple), and the value for C_H in a single solvent (Figure 1). While previous cyclic voltammetry experiments for **1**$^-$/**1** were performed using acetone as solvent, its acidity, the lack of a known C_H value for acetone, and the unavailability of pK_a values in acetone for organic conjugate acid−base pairs for use in evaluating the **1**$^-$/**2** equilibrium led us to seek an alternative. We chose THF, which lacks acidic functionality, and for which C_H is known to be 66 kcal/mol[12] and numerous organic acid−base pK_a values are available.[13]

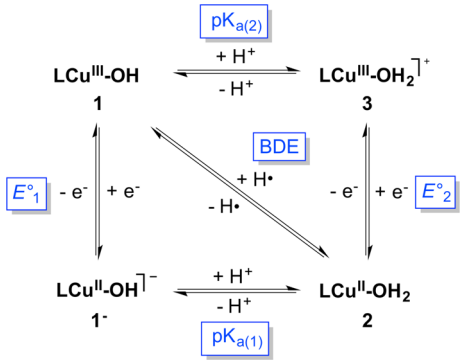

Figure 1. Square scheme relating the complexes examined in this work (L = *N*,*N*′-bis(2,6-diisopropylphenyl)-2,6-pyridinedicarboxamide).

The use of THF led to a complication, however, which we discovered upon observing that dissolution of brown crystals of **2** in THF resulted in a green solution. Working under the initial hypothesis that this color change indicated a ligand exchange reaction involving replacement of the H_2O ligand by solvent THF, solutions of **2** in THF were treated with a drying agent and the complex reisolated. The product was identified as the THF adduct LCu(THF) (**4**) on the basis of an X-ray crystal structure (Figure 2) and elemental analysis. Additional data

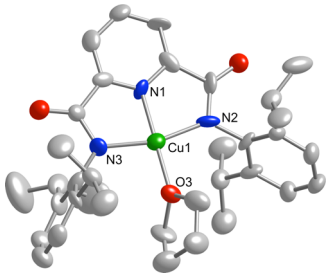

Figure 2. Representation of the X-ray crystal structure of LCu(THF) (**4**), showing all nonhydrogen atoms as 50% thermal ellipsoids. Selected interatomic distances (Å) and angles (deg): Cu1−N1, 1.883(13); Cu1−N2, 1.947(14); Cu1−N3, 1.948(11); Cu1−O3, 1.974(11); N1−Cu1−N2, 81.9(5); N1−Cu1−N3, 81.1(6); N2−Cu1−N3, 162.5(5); N1−Cu1−O3, 171.4(6); N2−Cu1−O3, 99.9(5); N3−Cu1−O3, 97.5(5).

indicated operation of an equilibrium between **2** and **4** in the presence of H_2O (eq 2). Thus, incremental addition of H_2O to solutions of **4** in THF resulted in a discernible shift of UV−vis spectral features (**2**, λ_{max} = 558 nm; **4**, λ_{max} = 577 nm; Figure 3,

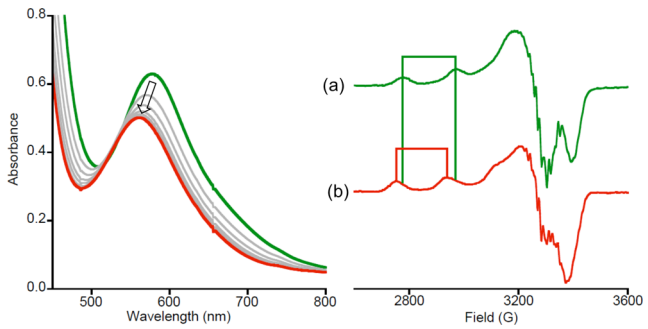

Figure 3. (left) UV−vis spectroscopic changes observed upon addition of increasing amounts of H_2O to solution of LCu(THF) (**4**) in THF (1 mM, green), culminating in the red spectrum (540 equiv of H_2O added). (right) X-band EPR spectra of (a) LCu(THF) (**4**) in THF, and (b) **4** in THF saturated with H_2O, recorded at 125 K, 9.3863 GHz. The brackets highlight the differences between the spectra in the $g_{||}$ region. Simulations and parameters are available in Figure S3.

left), the deconvolution and fitting of which enabled calculation of the equilibrium constant K_2 = 440 ± 20 (Figures S1−S2, Supporting Information). EPR spectral data were consistent with the UV−vis results; axial signals that were distinctly different were observed for pure **4** and for **4** in H_2O-saturated THF (Figure 3, right; simulations and parameters in Figure S3). Finally, the conversion of **4** to **2** upon addition of H_2O was evident in cyclic voltammograms (Figure 4). In dry THF, **4** exhibits a pseudoreversible wave with $E_{1/2}$ = 0.735 V vs Fc^+/Fc that we assign to the **4**/**4**$^+$ couple. Addition of H_2O causes this feature to decrease in intensity and a new wave to grow in with $E_{1/2}$ = 0.345 V; we assign this to the **2**/**2**$^+$ couple. Simulations of the voltammograms comprising both couples using

DOI: 10.1021/ja512014z
J. Am. Chem. Soc. 2015, 137, 1322−1329

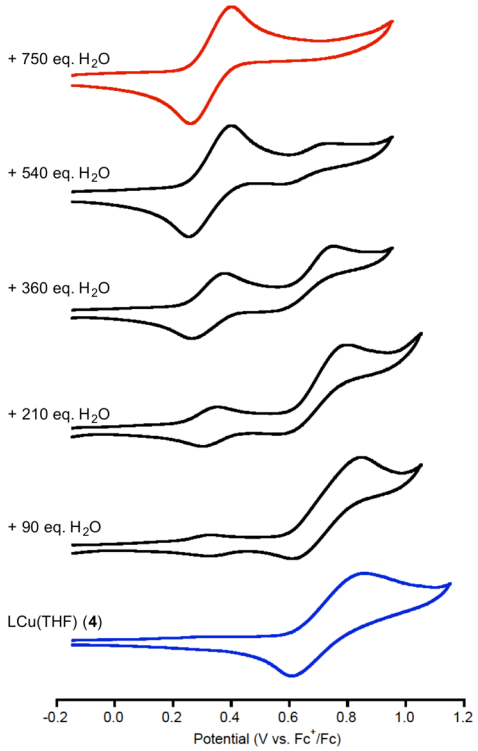

Figure 4. Cyclic voltammograms of LCu(THF) (**4**) in pure THF (blue, bottom) and in the presence of variable amounts of added H_2O, culminating in a wave assigned to LCu(H_2O) (**2**) (red, top). Conditions: THF, 0.2 M $TBAPF_6$, 200 mV/s.

DigiSim[14] gave $K_2 = 408 \pm 15$ (Figure S4), in close agreement with the value determined from the UV–vis titrations.

$$\underset{\mathbf{4}}{\mathrm{LCu(THF)}} + \mathrm{H_2O} \overset{K_2}{\rightleftharpoons} \underset{\mathbf{2}}{\mathrm{LCu(OH_2)}} + \mathrm{THF} \tag{2}$$

$$\underset{\mathbf{1}^-}{[\mathrm{LCuOH}]^-} + \mathrm{Et_3NH^+} + \mathrm{THF} \overset{K_3}{\rightleftharpoons} \underset{\mathbf{4}}{\mathrm{LCu(THF)}} + \mathrm{Et_3N} + \mathrm{H_2O} \tag{3}$$

$$\underset{\mathbf{1}^-}{[\mathrm{LCuOH}]^-} + \mathrm{Et_3NH^+} \overset{K_1}{\rightleftharpoons} \underset{\mathbf{2}}{\mathrm{LCu(H_2O)}} + \mathrm{Et_3N} \tag{4}$$

Importantly, the equilibrium in eq 2 had to be taken into account in efforts to determine the $pK_{a(1)}$ of **2**. The acid–base equilibrium between $\mathbf{1}^-$ and **2** was probed by titrating solutions of $\mathbf{1}^-$ in THF with known equivalents of triethylammonium triflate ([Et_3NH]OTf) and monitoring the changes in the UV–vis spectrum (Figure S5). On progressive addition of the acid, the absorption peak shifted from 597 nm ($\mathbf{1}^-$) to 577 nm (**4**), corresponding to the equilibrium eq 3. Multicomponent fitting of the data to determine K_3 (17 ± 1; Figures S6–S8) and use of K_2 and the known pK_a of Et_3NH^+ in THF (14.9 ± 1.7)[13] enabled calculation of K_1 and $pK_{a(1)} = 18.8 \pm 1.8$.

Cyclic voltammograms of $\mathbf{1}^-$ in THF with 0.2 M $TBAPF_6$ at 20 °C exhibited irreversible anodic waves at low scan rates ($E_{pa} \sim -0.03$ V vs Fc^+/Fc), but the return wave gained intensity as the scan rate was increased enabling determination of $E_{1/2} = -0.074$ V (Figures 5, left, and S9). This value agrees closely to that measured previously in acetone (−0.076 V).[5a] Importantly, using the values of $pK_{a(1)} = 18.8 \pm 1.8$, $E_{1/2} = -0.074$ V (vs Fc^+/Fc), and $C = 66$ kcal mol^{-1} in THF, we calculated a BDE

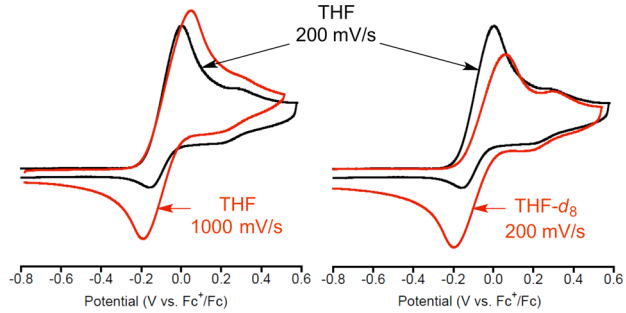

Figure 5. Cyclic voltammograms of $\mathbf{1}^-$ in THF (black, 200 mV/s) overlaid with one at higher scan rate (left, red, 1000 mV/s) or at same scan rate in THF-d_8 (right, red, 200 mV/s). Conditions: 0.2 M $TBAPF_6$, 20 °C.

for **2** of 90 ± 3 kcal mol^{-1}. Also, using the interdependence of the thermodynamic parameters in eq 1 and Figure 1, we estimate the value of $pK_{a(2)} = 11.7 \pm 2.2$.

Hypothesizing that the observed scan rate dependent electrochemical behavior in THF resulted from an ECE mechanism involving oxidation of $\mathbf{1}^-$ to **1** followed by chemical reaction of **1** with solvent C–H bonds to yield **2** (which itself undergoes reversible 1-electron oxidation), the cyclic voltammetry experiments were repeated using THF-d_8. Reversibility at lower scan rates was observed (Figure 5, right), and through simulations of the data in THF and THF-d_8 measured over the range of scan rates 50–1000 mV s^{-1} (Figure S10) the rate constants for the chemical reaction and the kinetic isotope effect were determined: $k_H = 0.114 \pm 0.004$ M^{-1} s^{-1}, $k_D = 0.0112 \pm 0.0003$ M^{-1} s^{-1}, $k_H/k_D = 10.2$. These results clearly support attack of **1** at the C–H(D) bonds of THF. Attempts to observe differences in rates of reaction with THF and THF-d_8 via UV–vis monitoring of the decay of **1** prepared chemically at −50 °C upon reaction of $\mathbf{1}^-$ with $FcPF_6$ revealed complicated decay kinetics that we have been unable to model. Nonetheless, different approximate $t_{1/2}$ values could be discerned ($t_{1/2}$(THF) = 230 s; $t_{1/2}$(THF-d_8) = 1080 s) that are consistent with attack of the THF C–H(D) bond by **1**.

HAT Reactivity. With the finding that **1** reacted with solvent THF at appreciable rates, we realized that evaluating the reactivity of **1** with substrates characterized by C–H bond strengths greater than that of THF (92 kcal mol^{-1})[11] would require use of a different medium. We had previously noted that **1** decayed quite slowly in 1,2-difluorobenzene (DFB; $k = 3.3 \times 10^{-7}$ s^{-1} at −25 °C).[5b] Consistent with the greater stability of **1** in DFB, cyclic voltammograms of $\mathbf{1}^-$ in DFB with 0.1 M $TBAPF_6$ at 20 °C exhibited pseudoreversible waves at scan rates 10–500 mV s^{-1} (Figure S11). For example, at the scan rate 200 mV s^{-1}, $E_{1/2} = -0.079$ V vs Fc/Fc^+, with $i_{pc}/i_{pa} \sim 0.9$ and $\Delta E_p = 156$ mV.

We then examined the reactivity of **1** prepared in DFB using $Fc[BAr^F{}_4]$[15] as oxidant at −25 °C with a variety of potential substrates spanning a BDE range of ~20 kcal mol^{-1} (DHA, fluorene, cyclohexene, diphenylmethane, toluene, THF, cyclohexane).[11] The reactions were monitored by UV–vis spectroscopy by following the decay of the intense absorption associated with **1** (0.1 mM) at 563 nm in the presence of excess substrate (0.005–8 M) at −25 °C. In all cases, the decay of **1** was accelerated in the presence of substrate, and pseudo-first-order rate constants were determined from initial rate data (~5–30% conversion). For all of the substrates except THF,

DOI: 10.1021/ja512014z
J. Am. Chem. Soc. 2015, 137, 1322–1329

linear fits of plots of these rate constants vs $[substrate]_0$ yielded second order rate constants k_2 (Figure S12).

For the case of THF, saturation behavior was observed (Figure 6 and S13). The simplest rate expression consistent

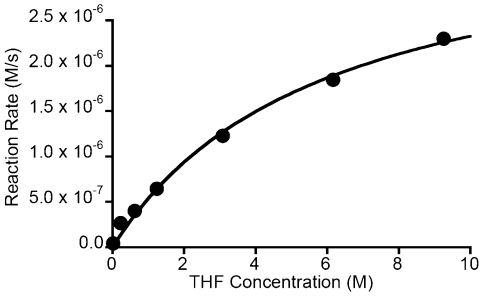

Figure 6. Plot of reaction rate vs $[THF]_0$ for the reaction of **1** with THF in DFB. The line is a fit to eq 5 (R = 0.997), yielding K_{eq} = 0.1688 M^{-1} and k_3 = 0.0371 s^{-1}.

with saturation kinetics is eq 5, to which the data fit well (R = 0.997), yielding K_{eq} = 0.1688 M^{-1} and k_3 = 0.0371 s^{-1}, where K_3 is the equilibrium constant for THF binding and k_3 is a second order rate constant for the HAT reaction (possible mechanistic interpretations are described in the Discussion section and in Scheme 2). We attempted to identify the final

Scheme 2

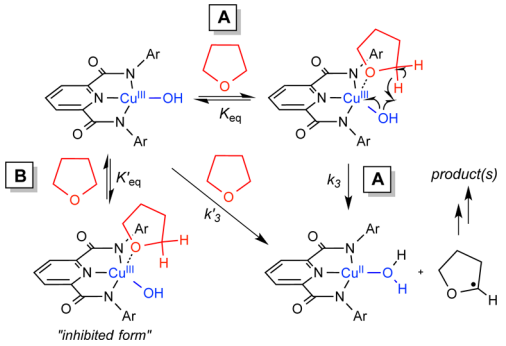

products of the reaction by allowing **1** to decay in THF and analyzing the volatile components by GC–MS. The data indicated formation of 2-hydroxytetrahydrofuran and γ-butyrolactone in variable yields (as high as ∼40 and 12%, respectively); neither of these compounds were present in control samples of THF solvent. The low and variable yields of these products are consistent with a HAT (radical) process.

$$\text{rate} = \frac{k_3[\mathbf{1}][\text{THF}]}{\frac{1}{K_{eq}} + [\text{THF}]} \quad (5)$$

Finally, the trends in rates of reaction as a function of substrate C–H bond strength were analyzed through a plot of $\log(k_2)$ or, for THF, $\log(k_3K_{eq})$ vs reported BDE values (Evans–Polanyi relation, Figure 7). The data are statistically corrected for the number of H atoms susceptible to abstraction (cf. 4 for cyclohexene, 12 for cyclohexane).

DISCUSSION

The thermodynamic parameters shown in the square scheme in Figure 1 were determined after taking into account the ligand substitution equilibrium involving $LCu(H_2O)$ (**2**) and LCu-

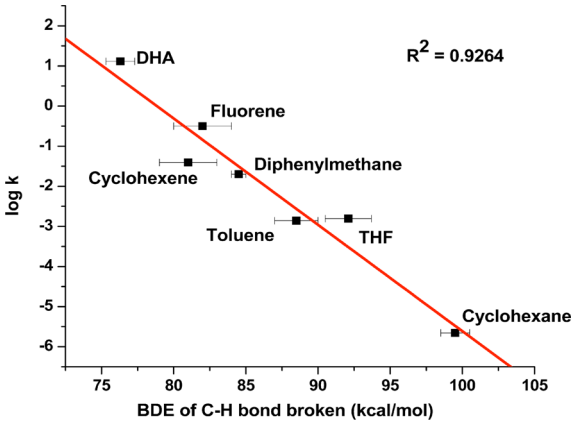

Figure 7. Plot of log k (where k is the second order rate constant k_2 or k_3K_{eq}) vs BDE for the reaction of **1** with the indicated substrates.

(THF) (**4**) (eq 2). These values are listed in Table 1 with others reported in the literature for various transition metal oxo/hydroxo complexes selected because of the availability of thermodynamic data and rate constants for reaction with DHA, and ordered by the BDE of the O–H bond formed upon reaction with substrates. Reported log k values for their reactions with DHA at 25 °C also are listed.

The evaluated pK_a of ∼19 for **2** indicates that $\mathbf{1}^-$ behaves as a very strong base in THF, with its basicity being comparable to that of certain phosphazenes and DBU (pK_a = 19.1).[13] It is noteworthy that in aprotic solvents having low permittivity like THF (ε = 7.39), interionic interactions have an accentuating effect on the pK_a values of neutral acids such as **2**.[19] For example, neutral phenols and benzoic acids have pK_a values in THF that are 8–13 units higher than in H_2O, e.g., for *p*-nitrophenol $pK_a(THF)$ = 21 vs $pK_a(H_2O)$ = 7.2.[19c] This effect has been attributed to a significant enhancement of the basicity of the conjugate base in the solvent with a low dielectric constant.[19a] Consequently, it is not surprising that $pK_{a(1)}$ is significantly higher than the reported pK_a values of other $Cu(OH_2)$ complexes which range from 7 to 13 in water.[20] In addition, the estimated $pK_{a(2)}$ of 11.7 supports our previous hypothesis that **1** is significantly basic,[5a] similar to the basicity of 2,4,6-trimethylpyridine (pK_a = 10.4 in THF).[13] These results differ from those recently reported for a putative $L'CuOH_2$ complex, where L′ is a related 2,6-pyridinedicarboxamide ligand with two pendant pyridine donors.[21] The pK_a of this species in H_2O was found to be 7, with an $E_{1/2}$ for the corresponding $L'Cu^{II}OH/L'Cu^{III}OH$ couple in H_2O of 1.29 V (vs SHE). The higher acidity and redox potential observed in this work relative to that which we have measured may arise from the effects of water solvent (polarity, hydrogen bonding) and/or differences in the coordination environment provided by L vs L′.

The high basicity of $\mathbf{1}^-$ is consistent with the dianionic, strongly electron donating characteristics of the supporting bis(arylamido)pyridine ligand, which also underly the low redox potential for the $\mathbf{1}/\mathbf{1}^-$ couple of −0.074 V vs Fc/Fc^+. These two parameters combine to yield an O–H BDE of 90 ± 3 kcal mol^{-1} for **2** that is among the highest compared to the metal-oxo/hydroxo complexes listed in Table 1. A similar conclusion is reached upon more extensive comparisons to literature data.[9a] For example, while BDE values of 92–100 kcal mol^{-1} have been estimated for some $[(porphyrin)Fe^{IV}OH]^{n+}$ complexes that are cited as particularly reactive cytochrome P450 analogues,[22] and a value of >91.6 kcal mol^{-1} was

DOI: 10.1021/ja512014z
J. Am. Chem. Soc. 2015, 137, 1322–1329

Table 1. Thermodynamic and Kinetic Parameters for 1 and Selected Metal Oxo/Hydroxo Complexes, Ordered by BDE of O−H Bond Formed upon Reaction with Substrates

complex	E°_1 (V)[a]	p$K_{a(1)}$	E^{0}_2 (V)[a]	p$K_{a(2)}$	BDE (kcal mol^{-1})	solvent	log k[d]	ref
LCuOH (1)	−0.074	18.8 ± 1.8	0.345	11.7 ± 2.2	90 ± 3	THF	2.27	5a, this work
$[Mn^{IV}H_3buea(O)]^{-}$[e]	−1.0	28.3	−0.18	15.0	89	DMSO	−1.59	8a, b
$[Fe^{IV}H_3buea(O)]^{-}$[e]	−0.9	25	−0.03	10	87	DMSO	–	8c
$[(bpy)_2(py)Ru^{IV}O]^{2+}$	<0.48[b]	>13	>1.6[b]	<0	84	H_2O	2.09	16
$[Fe^{III}(PY5)OMe]^{2+}$[f]	0.73	9.1	–	–	84	MeOH	−2.31	17
$[Mn^{IV}(Me_2EBC)(O)(OH)]^{+}$[g]			0.756	6.86	84	MeCN	−2.25	8h, i
$[Mn^{IV}(Me_2EBC)(OH)_2]^{2+}$	0.756	5.87	–	–	83	MeCN	−3.43	8h, i
$[(bpy)_2(py)Ru^{III}OH]^{2+}$	0.46[b]	10.6	1.02[b]	0.85	82	H_2O	–	16
$[Mn^{III}(PY5)OH]^{2+}$[f]	0.81	13	–	–	82	MeCN	−2.80	8f
$[MnO_4]^{-}$	0.56[b]	7.4	–	–	80	H_2O	−0.92	8g
$[Fe^{III}(PY5)OH]^{2+}$[f]	0.55	8.1	–	–	80	DMSO	−3.36	8e
$[L'_2Mn^{IV}(O)_2Mn^{III}L'_2]^{3+}$[h]	−0.01	14.6	–	–	79	MeCN	−2.81	8d
$[Fe^{IV}(O)(N_4Py)]^{2+}$[i]	0.24[c]	–	–	–	78	H_2O	1.25	18
$[Mn^{III}H_3buea(O)]^{2-}$[e]	−2.0	50.0	−1.51	28.3	77	DMSO	−0.53	8a, b
$[L'_2Mn^{III}(O)(OH)Mn^{III}L'_2]^{3+}$[h]	−0.03	11.5	–	–	75	MeCN	−3.38	8d
$[Fe^{III}H_3buea(O)]^{2-}$[e]	–	–	−1.79	25	66	DMSO	–	8c

[a]vs Fc/Fc$^+$ unless otherwise stated. [b]vs SHE. [c]vs SCE. [d]k = second order rate constant for the reaction with dihydroanthracene at 25 °C, either measured directly or extrapolated to this temperature from experimentally determined activation parameters. [e]H_6buea = tris[(N_3-*tert*-butylureayl)-*N*-ethylene]amine. [f]PY5 = 2,6-bis(bis(2-pyridyl)methoxymethane)pyridine. [g]Me_2EBC = 4,11-dimethyl-1,4,8,11-tetraazabicyclo[6.6.2]hexadecane. [h]L′ = phenanthroline. [i]N4Py = *N*,*N*-bis(2-pyridylmethyl)-bis(2-pyridyl)methylamine.

estimated for $(H_2O)_5CrOH^{2+}$,[23] most BDE values for metal complexes are <90 kcal mol^{-1}.

Complex **1** has a correspondingly high log k of 2.27 for HAT from DHA (BDE = 76.3 kcal mol^{-1}). High log k values of 2.09[16] for $[(bpy)_2(py)Ru^{IV}O]^{2+}$ and 1.25[18] for $[Fe^{IV}(O)(N_4Py)]^{2+}$ have been reported, but these complexes have lower BDE values of 84 and 78 kcal mol^{-1}, respectively. Interestingly, $[Mn^{IV}H_3buea(O)]^{-}$ affords a hydroxo product with a similar BDE to **2**, with a significantly lower redox potential (ΔE = −1 V) being approximately equally offset by much greater basicity (ΔpK_a = +10). Yet, despite the similar BDE values, $[Mn^{IV}H_3buea(O)]^{-}$ reacts with DHA at a much slower rate than **1** (Δlog k = −3.86). Among the factors potentially at play, we speculate that the H-bonding array surrounding the oxo unit in $[Mn^{IV}H_3buea(O)]^{-}$ inhibits substrate approach and slows PCET, and that the high reactivity of **1** derives both from its high BDE and a relatively high degree of steric access to the $[CuOH]^{2+}$ moiety. Caution in drawing further rate comparisons via BDE correlations is warranted by the fact that not all the complexes listed in Table 1 react via the same type of HAT process. For example, $[Mn^{IV}H_3buea(O)]^{-}$ reacts with DHA at a much slower rate than $[Mn^{III}H_3buea(O)]^{2-}$, which has a much lower driving force. The disparate results for these manganese compounds has been attributed to different mechanisms for their reactions with DHA (PCET for $[Mn^{IV}H_3buea(O)]^{-}$ vs stepwise proton transfer and then electron transfer for $[Mn^{III}H_3buea(O)]^{2-}$).

The high BDE for the O−H bond in **2** suggests that **1** should be capable of attacking strong C−H bonds at appreciable rates. Indeed, we found that **1** attacks the C−H bonds of THF (BDE = 92 kcal mol^{-1}) through analysis of CV data obtained in THF and THF-d_8. The observation of a large kinetic isotope effect of 10.2 at room temperature confirmed that C−H/D bond scission is rate determining. With the realization of the reactivity with solvent THF and the discovery that **1** was stabilized in DFB, experiments aimed at evaluating the reactivity of **1** with a wider array of possible substrates were enabled. Monitoring of the decay of **1** at −25 °C in DFB in the presence of excess amounts of substrates with C−H BDE values between 77 and 99 kcal mol^{-1} yielded second order rate constants that varied as a function of BDE value as shown in Figure 7. The observed linear dependence is congruent with similar plots for other oxidants,[7,8a−c,17] and supports a similar HAT pathway across the range of substrates. Much poorer correlations were observed in plots of log k vs pK_a or redox potential of the substrates (Figure S14). Particularly notable is the fact that **1** reacts with excess cyclohexane (BDE = 99 kcal mol^{-1}) at a rate approximately 10 times faster than self-decay, illustrating the power of **1** as an HAT reagent and, thus, its potential involvement in oxidation catalysis.

For the reaction of **1** in DFB with THF, saturation kinetics were observed, consistent with a mechanism (**A** in Scheme 2, parameters K_{eq} and k_3) involving rapid pre-equilibrium coordination of THF to the complex followed by rate-determining attack at a THF C−H bond. An alternative mechanism (**B**, parameters K'_{eq} and k'_3) is also consistent with the kinetic data. In this pathway, equilibrium THF binding to **1** results in inhibition, with intermolecular attack of the unbound form at an exogenous THF molecule (k'_3) being preferred. Since both pathways **A** and **B** yield the same experimentally observed rate law (eq 5), distinction between them is not possible with the data currently available.[24]

The attack of **1** at the C−H bonds of THF represents a rare example of oxidation of THF by a copper−oxygen species.[25] The reactions of a $[CuOH]^{2+}$ moiety with strong C−H bonds and, in particular, such bonds α to an ether functionality in THF, is notably relevant to proposals for glycoside cleavage by the copper-containing enzyme lytic polysaccharide monooxygenase (LPMO, Figure 8).[3h,26] The active site of LPMO contains a single copper ion in a tetragonal geometry with meridional binding of a monodentate His imidazolyl and a bidentate motif called a "histidine brace" comprising an imidazolyl and amino group. Two pathways for attack at the C−H bond of the saccharide unit have been considered for LPMO, involving either direct HAT from an initially formed $[CuOO]^{+}$ intermediate (Figure 8a) or 2e$^-$/2H$^+$ reduction of

DOI: 10.1021/ja512014z
J. Am. Chem. Soc. 2015, 137, 1322−1329

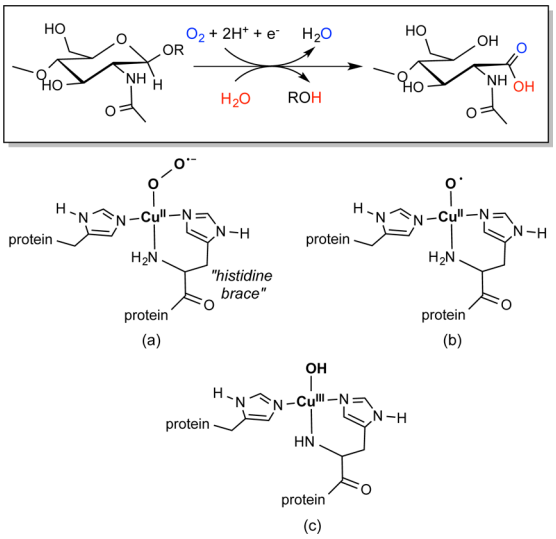

Figure 8. Glycosidic cleavage reaction catalyzed by lytic polysaccharide monooxygenase (adapted from ref 26a) and proposed structures for the active site oxidants (a–c).

this intermediate to yield a $[CuO]^+$ unit (b) that then reacts with the C–H bond of the substrate. Theoretical work suggests that the latter has a lower energy barrier.[3h]

We speculate on the basis of our findings that a $[CuOH]^{2+}$ species (c) should also be considered as a possible intermediate capable of attacking the α-C–H bond of substrate. Stabilization of the $[CuOH]^{2+}$ unit could result from deprotonation of the amino arm of the histidine brace; the resulting amide donor would mimic the carboxamide donors in **1** that lower its redox potential while at the same time raising the pK_a of the aquo ligand in **2**, resulting in a strong O–H BDE that underlies the high reactivity of the $[CuOH]^{2+}$ unit. This unit could form via protonation of the $[CuO]^+$ moiety from an external source, or via tautomerization involving the amino arm of the histidine brace (intermediate (b) to (c)).[6] Similar arguments might also apply to other powerful copper oxidants, such as that present in particulate methane monooxygenase (pMMO), the proposed active site of which also contains a histidine brace and also can be envisaged to involve a $[CuOH]^{2+}$ unit.

CONCLUSIONS

We have experimentally determined the BDE of the O–H bond in LCu(H_2O) (**2**) through evaluation of its pK_a and redox potential in THF, after defining the ligand substitution equilibrium between **2** and LCu(THF) (**4**) through UV–vis and EPR spectroscopy and cyclic voltammetry. Although **1** is a weak oxidant, the high basicity of $\mathbf{1}^-$ results in a high BDE of 90 ± 3 kcal mol^{-1} and a corresponding high rate of HAT from DHA. Analysis of CV data revealed that **1** reacts with solvent THF/THF-d_8 via attack at its C–H(D) bonds with an isotope effect of 10.2. Substrates with a variety of C–H bond strengths were found to react with **1** in DFB solution, and a linear relationship between log k and BDE for the substrate C–H bond was found. Saturation kinetics were observed for THF as substrate in DFB, consistent with a mechanism involving pre-equilibrium binding of THF followed by intramolecular C–H bond activation, or one involving inhibition of intermolecular attack through binding of THF to **1**. The discovery that **1** attacks strong C–H bonds in a variety of substrates attests to its viability as a possible reactive species in oxidation catalysis, including by copper enzymes, with its high O–H BDE being a key basis for its HAT capabilities.

EXPERIMENTAL SECTION

Materials and Methods. All solvents and reagents were purchased from commercial sources and used as received unless otherwise noted. Elemental analyses were performed by Robertson Microlit Laboratory (Ledgewood, NJ). Tetrahydrofuran was dried over sodium/benzophenone and vacuum distilled. Acetonitrile, 1,2-difluorobenzene, cyclohexane and cyclohexene were dried over calcium hydride and vacuum distilled. Toluene, pentanes, and diethyl ether were passed through solvent purification columns (Glass Contour, Laguna, California). All solvents were stored over 3 Å molecular sieves for at least 4 h prior to use. Metal complexes were synthesized and manipulated in a Vacuum Atmospheres glovebox under an inert atmosphere of nitrogen or by using standard Schlenk-line techniques. HPLC grade water was degassed by bubbling in N_2 for 15 min before it was used for the titrations and electrochemistry experiments. UV–vis spectra were obtained using an HP8453 (190–1100) diode array spectrophotometer. Cyclic voltammograms were recorded using an EC Epsilon potentiostat from BASi, a glassy-carbon working electrode, and a Ag^+/Ag reference electrode; they were referenced internally using decamethylferrocene. In particular, the electrochemistry for $\mathbf{1}^-$ in THF was recorded using both a glassy-carbon and Pt-working electrode to confirm that the nature of the electrode surface does not affect the reactivity of the generated species. The final potentials were then converted vs the standard Fc^+/Fc couple using standard conversion factors.[27] The experimental cyclic voltammograms were modeled using the DigiSim 3.03b software package from BASi. For X-ray diffraction measurements, data collection was done using Cu Kα radiation and a Bruker D8 Photon 100 CMOS diffractometer using normal parabolic mirrors as monochromators. EPR spectra were recorded on a CW X-band EleXsys E500 EPR spectrometer and simulations were performed using Bruker SimFonia software (version 1.25). All GC–MS experiments were conducted on an Agilent Technologies 7890A GC system and 5975C VL MSD. The GC column was a HP-5 ms with dimensions 30 m × 0.25 mm. The standard method used for all runs involved an initial oven temperature of 50 °C (held for 2 min) followed by a 20 °C min^{-1} ramp to 70 °C (held for 6 min), followed by a final 20 °C min^{-1} ramp to 230 ∘C (held for 15 min). The flow rate was 1 mL/min and inlet temperature was 250 °C. The ligand H_2L and the corresponding metal complexes $[Bu_4N][LCuOH]$ ($\mathbf{1}^-$) and **2** were synthesized using previously reported procedures.[5a] $[Et_3NH]OTf$ was prepared by adding AgOTf (257 mg, 1 mmol) to $[Et_3NH]Cl$ (137 mg, 1 mmol) dissolved in dry acetonitrile (5 mL) in the glovebox. After stirring for 20 min, the precipitated AgCl was removed by filtration and solvent was removed from the filtrate in vacuo to yield the product as a colorless viscous liquid (210 mg, 85%). ^{1}H NMR (DMSO-d_6): δ 1.15 (t, J = 7.2 Hz, 9H), 3.09 (m, 6H), 8.84 (s, 1H) ppm.

Synthesis of LCu(THF) (4). A solution of **2** (200 mg, 0.35 mmol) in dry THF (10 mL) was stirred over 3 Å molecular sieves for 3 h. The mixture was filtered to remove the pulverized molecular sieves and the filtrate was evaporated to yield a green colored solid. The isolated solid was then dissolved in THF/Et_2O (1:1 by volume, 10 mL) and stirred for a further 30 min, following which the solvents were removed in vacuo to yield the product as a fine powdery green solid (160 mg, 75%). Small prismatic green crystals for analysis by X-ray crystallography were grown by vapor diffusion of pentanes into a THF solution of the solid at −19 °C. UV–vis (THF, 25 °C) λ_{max}, nm (ε): 397 (2700), 577 (630). Anal. Calculated for $C_{35}H_{45}CuN_3O_3$: C, 67.88; H, 7.32; N, 6.79. Found: C, 67.63; H, 7.67; N, 7.27.

Reactions of LCu(THF) (4) with H_2O. *UV–Vis.* To a solution of **4** in dry THF (3 mL, 1 mM) in a cuvette under nitrogen at room temperature was added HPLC grade degassed water in 5 μL increments. UV–vis spectra were recorded (Figure 3) and simulated using two separate Lorentzian functions centered at 577 nm (for **4**) and 558 nm (for **2**) via the program Fityk (0.9.8). The extinction

DOI: 10.1021/ja512014z
J. Am. Chem. Soc. 2015, 137, 1322–1329

coefficient for **2** in THF was estimated to be ~500 M^{-1} cm^{-1} based on the absorbance at the end of the titration assuming complete conversion of **4** to **2** (evidenced by no further shifts and only dilution effects beyond addition of 540 equiv of water). Representative deconvolution traces and linearized titration plots are depicted in Figures S1−S2.

EPR. To a solution of **4** in dry THF (0.6 mL, 5 mM) in a cuvette under nitrogen at room temperature was added 2.3 mL dry THF and 0.1 mL degassed HPLC grade water so as to generate a 1 mM solution of **2** in THF (in the presence of excess water). The formation of the species was confirmed by UV−vis spectroscopy and then this solution was used for EPR measurements. EPR measurements of **4** were taken on a separately prepared 1 mM solution of **4** in dry THF. All EPR spectra were recorded at 125 K, 9.3863 GHz.

Cyclic Voltammetry. To a solution of **4** in dry degassed THF (6 mL, 3 mM; 0.2 M $TBAPF_6$) under argon, incremental amounts of degassed HPLC grade water were added and the cyclic voltammogram subsequently recorded. The voltammograms at every titration point were then simulated using two reversible redox couples for $\mathbf{4}/\mathbf{4}^+$ and $\mathbf{2}/\mathbf{2}^+$ assuming an equilibrium between **4** and **2** (details in Supporting Information).

Titration of $[Bu_4N][LCuOH]$ ($\mathbf{1}^-$) with $[Et_3NH]OTf$. To a solution of $\mathbf{1}^-$ in dry THF (2 mL, 1 mM) in a cuvette under nitrogen at room temperature was added a solution of $[Et_3NH]OTf$ in THF (5 mM) in 0.05 mL increments. UV−vis spectra were recorded (Figure S5) and simulated to determine the relative amounts of the species in solution as described above, here using a Gaussian function centered at 597 nm ($\mathbf{1}^-$) and a Lorentzian function centered at 577 nm (**4**) (Figure S6). Representative deconvolution traces and linearized titration plots are depicted in Figures S7−S8. The concentrations of $\mathbf{1}^-$ and **4** were determined using the extinction coefficients 350 ± 3 M^{-1} cm^{-1} and 630 ± 12 M^{-1} cm^{-1}, respectively, determined from independently analyzed Beers' Law plots.

Procedure for Kinetic Studies with Different Substrates in DFB. To a 1.8 mL solution of a known concentration of the substrate in DFB in a cuvette, 0.1 mL of a 2 mM solution of $\mathbf{1}^-$ was added under nitrogen and the contents were cooled to −25 °C for 10 min. To this solution 0.1 mL of a 2 mM solution of $Fc[BAr^F{}_4]$[15] in DFB was added, resulting in the immediate appearance of a feature at 563 nm associated with formation of **1**. Subsequent decay of the absorption peak at 563 nm was monitored over time by UV−vis spectroscopy. For all substrates except cyclohexane and THF, the decay trace of the peak was fit to a single exponential decay function to obtain the pseudo-first-order rate constant (k_{obs}). For cyclohexane and THF, the method of initial rates was used, whereby the slope of the linear fit of the decay trace monitored over initial 5% of the reaction was used to determine the pseudo-first-order rate constant (cyclohexane) or rate (THF). For all substrates except THF, linear fitting of plots of k_{obs} vs the substrate concentration afforded the second order rate constant (Figure S12). For THF, the plot of initial rate vs the concentration of THF was fit to eq 5.

Product Analysis of THF Oxidations. To a solution of $\mathbf{1}^-$ (8 mg, 0.01 mmol) dissolved in dry THF (0.9 mL) at −25 °C under an argon atmosphere was added a solution of 10 mg of $Fc[BAr^F{}_4]$ (10 mg, 0.01 mmol) in dry THF (0.1 mL), which resulted in the immediate formation of an intense purple solution. Upon stirring at −25 °C for 30 min the solution turned green, after which it was warmed to room temperature and stirred for an additional 5 min to ensure complete reaction. The volatiles were collected by vacuum distillation and analyzed by GC−MS using octane as an internal standard according to a previously reported protocol.[25a] The data indicated the presence of 2-hydroxytetrahydrofuran (~37% yield) and γ-butyrolactone (12% yield), with signifianct variability in yields in repeated runs. Data from control experiments using only THF did not show these products.

■ ASSOCIATED CONTENT

Supporting Information

Spectroscopic, CV, and kinetic data and fits (PDF) and X-ray crystallographic information (CIF). This material is available free of charge via the Internet at http://pubs.acs.org.

■ AUTHOR INFORMATION

Corresponding Author

wtolman@umn.edu

Notes

The authors declare no competing financial interest.

■ ACKNOWLEDGMENTS

We thank the NIH (GM47365) for financial support of this research. X-ray diffraction experiments were performed using a crystal diffractometer acquired through NSF-MRI Award CHE-1229400. The EPR spectroscopy experiments were performed at the Biophysical Spectroscopy Center in the University of Minnesota Department of Biochemistry, Molecular Biology and Biophysics, and we thank Gereon M. Yee and Benjamin D. Neisen for assistance with these experiments.

■ REFERENCES

(1) Solomon, E. I.; Heppner, D. E.; Johnston, E. M.; Ginsbach, J. W.; Cirera, J.; Qayyum, M.; Kieber-Emmons, M. T.; Kjaergaard, C. H.; Hadt, R. G.; Tian, L. *Chem. Rev.* **2014**, *114*, 3659−3853.

(2) Selected reviews: (a) Mirica, L. M.; Ottenwaelder, X.; Stack, T. D. P. *Chem. Rev.* **2004**, *104*, 1013−1045. (b) Lewis, E. A.; Tolman, W. B. *Chem. Rev.* **2004**, *104*, 1047−1076. (c) Himes, R. A.; Karlin, K. D. *Curr. Opin. Chem. Biol.* **2009**, *13*, 119−131. (d) Itoh, S. *Curr. Opin. Chem. Biol.* **2006**, *10*, 115−122. (e) Cramer, C. J.; Tolman, W. B. *Acc. Chem. Res.* **2007**, *40*, 601−608. (f) Fukuzumi, S.; Karlin, K. D. *Coord. Chem. Rev.* **2013**, *257*, 187−195. (g) Haack, P.; Limberg, C. *Angew. Chem., Int. Ed.* **2014**, *53*, 1−13.

(3) Illustrative references: (a) Chen, P.; Solomon, E. I. *J. Am. Chem. . Soc.* **2004**, *126*, 4991−5000. (b) Decker, A.; Solomon, E. I. *Curr. Opin. Chem. Biol.* **2005**, *9*, 152−163. (c) Yoshizawa, K.; Kihara, N.; Kamachi, T.; Shiota, Y. *Inorg. Chem.* **2006**, *45*, 3034−3041. (d) Crespo, A.; Marti, M. A.; Roitberg, A. E.; Amzel, L. M.; Estrin, D. A. *J. Am. Chem. Soc.* **2006**, *128*, 12817−12828. (e) Gherman, B. F.; Heppner, D. E.; Tolman, W. B.; Cramer, C. J. *J. Biol. Inorg. Chem.* **2006**, *11*, 197−205. (f) Huber, S. M.; Ertem, M. Z.; Aquilante, F.; Gagliardi, L.; Tolman, W. B.; Cramer, C. J. *Chem.—Eur. J.* **2009**, *15*, 4886−4895. (g) Dietl, N.; van der Linde, C.; Schlangen, M.; Beyer, M. K.; Schwarz, H. *Angew. Chem., Int. Ed.* **2011**, *50*, 4966−4969. (h) Kim, S.; Ståhlberg, J.; Sandgren, M.; Paton, R. S.; Beckham, G. T. *Proc. Natl. Acad. Sci. U. S. A.* **2014**, *111*, 149−154. (i) Conde, A.; Vilella, L.; Balcells, D.; Díaz-Requejo, M. M.; Lledós, A.; Pérez, P. J. *J. Am. Chem. Soc.* **2013**, *135*, 3887−3896.

(4) (a) Shiota, Y.; Yoshizawa, K. *Inorg. Chem.* **2009**, *48*, 838−845. (b) Shiota, Y.; Juhász, G.; Yoshizawa, K. *Inorg. Chem.* **2013**, *52*, 7907−7917. (c) Balasubramanian, R.; Smith, S. M.; Rawat, S.; Yatsunyk, L. A.; Stemmler, T. L.; Rosenzweig, A. C. *Nature* **2010**, *465*, 115−119. (d) Culpepper, M. A.; Rosenzweig, A. C. *Crit. Rev. Biochem. Mol. Biol.* **2012**, *47*, 483−492.

(5) (a) Donoghue, P. J.; Tehranchi, J.; Cramer, C. J.; Sarangi, R.; Solomon, E. I.; Tolman, W. B. *J. Am. Chem. Soc.* **2011**, *133*, 17602−17605. (b) Tehranchi, J.; Donoghue, P. J.; Cramer, C. J.; Tolman, W. B. *Eur. J. Inorg. Chem.* **2013**, *2013*, 4077−4084.

(6) Such protonation of a $[CuO]^+$ species has been proposed: Buijs, W.; Comba, P.; Corneli, D.; Pritzkow, H. *J. Organomet. Chem.* **2002**, *641*, 71−80.

(7) (a) Borovik, A. S. *Chem. Soc. Rev.* **2011**, *40*, 1870−1874. (b) Green, M. T.; Dawson, J. H.; Gray, H. B. *Science* **2004**, *304*, 1653−1656. (c) Lansky, D. E.; Goldberg, D. P. *Inorg. Chem.* **2006**, *45*, 5119−5125. (d) Sastri, C. V.; Lee, J.; Oh, K.; Lee, Y. J.; Lee, J.; Jackson, T. A.;

DOI: 10.1021/ja512014z
J. Am. Chem. Soc. 2015, 137, 1322−1329

Ray, K.; Hirao, H.; Shin, W.; Halfen, J. A.; Kim, J.; Que, L.; Shaik, S.; Nam, W. *Proc. Natl. Acad. Sci. U. S. A.* **2007**, *104*, 19181−19186.
(8) (a) Gupta, R.; Borovik, A. S. *J. Am. Chem. Soc.* **2003**, *125*, 13234−13242. (b) Parsell, T. H.; Yang, M.; Borovik, A. S. *J. Am. Chem. Soc.* **2009**, *131*, 2762−2763. (c) Usharani, D.; Lacy, D. C.; Borovik, A. S.; Shaik, S. *J. Am. Chem. Soc.* **2013**, *135*, 17090−17104. (d) Wang, K.; Mayer, J. M. *J. Am. Chem. Soc.* **1997**, *119*, 1470−1471. (e) Goldsmith, C. R.; Stack, T. D. P. *Inorg. Chem.* **2006**, *45*, 6048−6055. (f) Goldsmith, C. R.; Cole, A. P.; Stack, T. D. P. *J. Am. Chem. Soc.* **2005**, *127*, 9904−9912. (g) Gardner, K. A.; Kuehnert, L. L.; Mayer, J. M. *Inorg. Chem.* **1997**, *36*, 2069−2078. (h) Yin, G.; Danby, A. M.; Kitko, D.; Carter, J. D.; Scheper, W. M.; Busch, D. H. *J. Am. Chem. Soc.* **2007**, *129*, 1512−1513. (i) Yin, G.; Danby, A. M.; Kitko, D.; Carter, J. D.; Scheper, W. M.; Busch, D. H. *J. Am. Chem. . Soc.* **2008**, *130*, 16245−16253.
(9) (a) Warren, J. J.; Tronic, T. A.; Mayer, J. M. *Chem. Rev.* **2010**, *110*, 6961−7001. (b) Mayer, J. M. *Acc. Chem. Res.* **2011**, *44*, 36−46. (c) Mayer, J. M. *Acc. Chem. Res.* **1998**, *31*, 441−450. (d) Mayer, J. M.; Rhile, I. J. *Biochim. Biophys. Acta* **2004**, *1655*, 51−58. (e) Mayer, J. M. *Annu. Rev. Phys. Chem.* **2004**, *55*, 363−390. (f) Bordwell, F. G.; Cheng, J. P.; Harrelson, J. A., Jr. *J. Am. Chem. Soc.* **1988**, *110*, 1229−1231.
(10) We assume that entropic effects are negligible in our system so that the use of BDE and C_H rather than BDFE and C_G is warranted. Recognizing that this assumption is not always valid,[7a] we nonetheless lack entropy data for our system that would shed light on this question.
(11) *Handbook of Bond Dissociation Energies in Organic Compounds*; Luo, Y., Ed.; CRC Press: New York, 2002; pp 11−93.
(12) (a) Tilset, M. In *Electron Transfer in Chemistry*; Balzani, V., Ed.; Wiley-VCH: Weinheim, Germany, 2001; pp 677−713. (b) Cappellani, E. P.; Drouin, S. D.; Jia, G.; Maltby, P. A.; Morris, R. H.; Schweitzer, C. T. *J. Am. Chem. Soc.* **1994**, *116*, 3375−3388.
(13) Garrido, G.; Koort, E.; Ràfols, C.; Bosch, E.; Rodima, T.; Leito, I.; Rosés, M. *J. Org. Chem.* **2006**, *71*, 9062−9067.
(14) DigiSim 3.03b from BASi Analytical instruments.
(15) BAr^F_4 represents $[B[3,5\text{-}(CF_3)_2C_6H_3]_4]^-$. This anion was used preferentially over the conventional PF_6^- because of enhanced solubility and stability. $Fc[BAr^F_4]$ was synthesized using the reported procedure: Bras, J. L.; Jiao, H.; Meyer, W. E.; Hampel, F.; Gladysz, J. A. *J. Organomet. Chem.* **2000**, *616*, 54−66.
(16) (a) Moyer, B. A.; Meyer, T. J. *Inorg. Chem.* **1981**, *20*, 436−444. (b) Lebeau, E. L.; Binstead, R. A.; Meyer, T. J. *J. Am. Chem. Soc.* **2001**, *123*, 10535−10544. (c) Bryant, J. R.; Mayer, J. M. *J. Am. Chem. Soc.* **2003**, *125*, 10351−10361.
(17) Goldsmith, C. R.; Jonas, R. T.; Stack, T. D. P. *J. Am. Chem. Soc.* **2002**, *124*, 85−98.
(18) Wang, D.; Zhang, M.; Bühlmann, P.; Que, L., Jr. *J. Am. Chem. Soc.* **2010**, *132*, 7638−7644.
(19) (a) Abdur-Rashid, K.; Fong, T. P.; Greaves, B.; Gusev, D. G.; Hinman, J. G.; Landau, S. E.; Lough, A. J.; Morris, R. H. *J. Am. Chem. Soc.* **2000**, *122*, 9155−9171. (b) Barbosa, J.; Barrón, D.; Bosch, E.; Rosés, M. *Anal. Chim. Acta* **1992**, *265*, 157−165. (c) Barrón, D.; Bosch, E.; Rosés, M. *Anal. Chim. Acta* **2000**, *403*, 339−347.
(20) Gilson, R.; Durrant, M. C. *Dalton Trans.* **2009**, 10223−10230 and references therein.
(21) Coggins, M. K.; Zhang, M.; Chen, Z.; Song, N.; Meyer, T. J. *Angew. Chem., Int. Ed.* **2014**, *53*, 12226−12230.
(22) Bell, S. R.; Groves, J. T. *J. Am. Chem. Soc.* **2009**, *131*, 9640−9641.
(23) Bakac, A. *J. Am. Chem. Soc.* **2000**, *122*, 1092−1097.
(24) We acknowledge the possibility that the rate decrease at rather high $[THF]_0$ may also be due to an (ill-defined) effect of the change in reaction medium.
(25) (a) Zhang, C. X.; Liang, H.-C.; Kim, E.-I.; Shearer, J.; Helton, M. E.; Kim, E.; Kaderli, S.; Incarvito, C. D.; Zuberbühler, A. D.; Rheingold, A. L.; Karlin, K. D. *J. Am. Chem. Soc.* **2003**, *125*, 634−635. (b) Luckay, R. C.; Sheng, X.; Strasser, C. E.; Raubenheimer, H. G.; Safin, D. A.; Babashkina, M. G.; Klein, A. *New J. Chem.* **2010**, *34*, 2835. (c) Halvagar, M. R.; Tolman, W. B. *Inorg. Chem.* **2013**, *52*, 8306−8308.
(26) (a) Vaaje-Kolstad, G.; Westereng, B.; Horn, S. J.; Liu, Z.; Zhai, H.; Sorlie, M.; Eijsink, V. G. H. *Science* **2010**, *330*, 219−222. (b) Quinlan, R. J.; Sweeney, M. D.; Leggio, L. L.; Otten, H.; Poulsen, J.-C. N.; Johansen, K. S.; Krogh, K. B. R. M.; Jørgensen, C. I.; Tovborg, M.; Anthonsen, A.; Tryfonad, T.; Walter, C. P.; Dupree, P.; Xu, F.; Davies, G. J.; Walton, P. H. *Proc. Natl. Acad. Sci. U. S. A.* **2011**, *108*, 15079−15084. (c) Hemsworth, G. R.; Henrissat, B.; Davies, G. J.; Walton, P. H. *Nat. Chem. Biol.* **2014**, *10*, 122−126. (d) Hemsworth, G. R.; Davies, G. J.; Walton, P. H. *Curr. Opin. Struct. Biol.* **2013**, *23*, 660−668. (e) Beeson, W. T.; Phillips, C. M.; Cate, J. H. D.; Marletta, M. A. *J. Am. Chem. Soc.* **2012**, *134*, 890−892. (f) Hemsworth, G. R.; Taylor, E. J.; Kim, R. Q.; Gregory, R. C.; Lewis, S. J.; Turkenburg, J. P.; Parkin, A.; Davies, G. J.; Walton, P. H. *J. Am. Chem. Soc.* **2013**, *135*, 6069−6077. (g) Kjaergaard, C. H.; Qayyum, M. F.; Wong, S. D.; Xu, F.; Hemsworth, G. R.; Walton, D. J.; Young, N. A.; Davies, G. J.; Walton, P. H.; Johansen, K. S.; Hodgson, K. O.; Hedman, B.; Solomon, E. I. *Proc. Natl. Acad. Sci. U. S. A.* **2014**, *111*, 8797−8802.
(27) Noviandri, I.; Brown, K. N.; Fleming, D. S.; Gulyas, P T.; Lay, P. A.; Masters, A. F.; Philips, L. *J. Phys. Chem. B* **1999**, *103*, 6713−6722.

DOI: 10.1021/ja512014z
J. Am. Chem. Soc. 2015, 137, 1322−1329